Journal of Power Sources 197 (2012) 12–19

Contents lists available at SciVerse ScienceDirect

Journal of Power Sources

journal homepage: www.elsevier.com/locate/jpowsour

Effect of $La_{0.1}Sr_{0.9}Co_{0.5}Mn_{0.5}O_{3-\delta}$ protective coating layer on the performance of $La_{0.6}Sr_{0.4}Co_{0.8}Fe_{0.2}O_{3-\delta}$ solid oxide fuel cell cathode

Ping-Yi Chou, Chun-Jing Ciou, Yu-Chen Lee, I-Ming Hung*

Yuan Ze Fuel Cell Center, Department of Chemical Engineering and Materials Science, Yuan Ze University, No. 135, Yuan-Tung Road, Chungli, Taoyuan 320, Taiwan

ARTICLE INFO

Article history:
Received 22 August 2011
Accepted 9 September 2011
Available online 19 September 2011

Keywords:
Solid oxide fuel cell
Interconnect
Protective coating layer
Chromium poison
Cathode

ABSTRACT

This study investigates the interface reactivity between $La_{0.1}Sr_{0.9}Co_{0.5}Mn_{0.5}O_{3-\delta}$ (LSCM) protective coating layer and Crofer22H interconnects. Additionally, we report the mechanism of Cr poisoning of the $La_{0.6}Sr_{0.4}Co_{0.8}Fe_{0.2}O_{3-\delta}$ (LSCF) cathode's electrochemical properties. The phase, chemical composition, and element distribution of compounds formed at the LSCM-Crofer22H interface are analyzed by X-ray diffraction (XRD) and electron dispersive microscopy (EDS). After heat treatment at 800 °C for 100 h, the LSCM/Crofer22H sample contains $SrCrO_3$, a compound with good conductivity; the area specific resistance (ASR) for the LSCM/Crofer22H interconnect is approximately 17–40 mΩ cm^2. We found that the amount of $(Mn_{0.98}Fe_{0.02})(Mn_{0.02}Fe_{0.48}Cr_{1.5})O_4$, Cr_3O_4, and $(Fe,Cr)_2O_3$ oxides form in LSCF/LSCM/Crofer22H is significantly less than that in LSCF/Crofer22H. LSCF conductivity after heating at 800 °C for 100 h, is notably higher when in contact with LSCM/Crofer22H than it is when in contact with Crofer22H. These results demonstrate that the LSCM protective coating prevents LSCF cathode poisoning by Cr evaporated from the Corfer22H interconnects.

1. Introduction

Solid oxide fuel cells (SOFCs) efficiently produce electricity in a silent and environmentally friendly manner. SOFCs offer many advantages such as high power density, low pollution, and fuel source flexibility by using hydrocarbon fuels [1]. However, SOFC high operating temperatures cause cathode poisoning by chromium species that diffuse from the metal interconnector, and thus, material compatibility between the electrolyte, electrode, and interconnector are significant challenges. The SOFC interconnect must exhibit high electrical conductivity, low ionic conductivity, high mechanical strength, and stability under both wet hydrogen and air atmospheres. The $(La,Sr,Ca)(Cr,Mg)O_3$-based perovskite ceramics were originally used as the interconnect; this material offered a coefficient of thermal expansion (CTE) similar to that of other components, and was stable against oxidation at high temperatures. However, its manufacture is difficult and expensive. Recently, SOFC operating temperatures decreased to an intermediate temperature range of 600–800 °C, and thus, metal interconnects now have the potential to supplant the traditional ceramic interconnect. Metal interconnects offer many advantages over the ceramic interconnect, including (i) low cost; (ii) mechanical stability; (iii) provide an effective barrier to gas; (iv) good conductivity; (v) high thermal conductivity; and (vi) ease of manufacture. Additionally, the metal interconnect must exhibit excellent high-temperature corrosion resistance. Among the available metal alloy interconnect materials, ferritic stainless steels are good candidates because of the high electrical conductivity oxide thin film that forms on their surface, ease of manufacture, matched CTE, and low cost. However, high Cr volatility results in poisoning of the SOFC cathode electrochemical properties. Crofer22 series alloys have been widely applied as an SOFC interconnect with low area specific resistance (ASR) after long operating times [2–5], due to the formation of $(Mn,Cr)_3O_4$ and other Cr-rich compounds. However, Cr volatility still causes degradation in cell performance. ThyssenKrupp VDM recently developed Crofer22H, a new material with better mechanical strength and creep characteristics at high temperature than those of Crofer22 APU. Crofer22 APU required vacuum casting, while Crofer22H can be produced in air. The Crofer22H elemental chemical composition is shown in Table 1.

The chromium content of a metal alloy diffuses toward the interconnect–cathode interface where Cr_2O_3 is formed. The Cr_2O_3 can react with water to form $CrO_2(OH)_2$, which then diffuses into the cathode electrode to form Cr_2O_3 at the cathode–electrolyte interface. The formation of Cr_2O_3 on both sides of the cathode, between interconnect and electrolyte [6–9], prohibits electron flow into the cathode, and causes an apparent increase in cathode resistance. In addition, the oxygen reduction reaction (ORR) is prohibited due to reaction of electrons with gaseous $CrO_2(OH)_2$ to form Cr_2O_3; this significantly decreases the rate of oxygen ion

* Corresponding author. Tel.: +886 3 4638800x2569; fax: +886 3 4630634.
E-mail address: imhung@saturn.yzu.edu.tw (I.-M. Hung).

0378-7753/$ – see front matter © 2011 Elsevier B.V. All rights reserved.
doi:10.1016/j.jpowsour.2011.09.017

Table 1
Chemical composition of Crofer22H.

wt.%	C	S	Cr	Mn	Si	Ti	Nb	Cu	Fe	P	Al	W	La
Crofer22H	0.007	<0.002	22.93	0.43	0.21	0.07	0.51	0.02	73.26	0.014	0.02	1.94	0.08

transport to the electrolyte. This process results in an increase in electrical resistance, and decreases the cathode's oxygen catalytic activity, causing SOFC performance and stability to decrease gradually [10–12].

To prevent Cr in the metal interconnect from poisoning the cathode, a protective oxide coating on the metal interconnect surface may provide high electrical conductivity with low Cr diffusion at high temperatures. Many types of protection layer materials are in use, including $La_{0.9}Sr_{0.1}MnO_3$ [13], $La_{0.6}Sr_{0.4}Co_{0.2}Fe_{0.8}O_3$ [14], $La_{0.8}Sr_{0.2}CoO_3$ [5], Ag-perovskite [15], yttria/cobalt or yttria/gold [16], $CuMn_{1.8}O_4$ [17], and Y or Co [18]. Among these protection layer materials, $(Mn,Co)_3O_4$-based materials are most widely used [19–23]. However, the CTE of $(Mn,Co)_3O_4$ is about $11.5 \times 10^{-6}\,K^{-1}$ [24], which is less than that of the $La_xSr_{1-x}Co_yFe_{1-y}O_{3-\delta}$ (LSCF) cathode, with a CTE of $15–19 \times 10^{-6}\,K^{-1}$ [20]. A CTE mismatch between cathode protection layers may cause cracking, and cause unstable SOFC performance after a long period of operation.

$La_{0.1}Sr_{0.9}Co_{0.5}Mn_{0.5}O_{3-\delta}$ (LSCM) is a potential material for the protection layer because it has high electrical conductivity and matched CTE, similar structure, and electrochemical composition to the LSCF cathode. Perovskite LSCM has CTE values of approximately $15.6 \times 10^{-6}\,K^{-1}$ [20], which is close to that of the LSCF cathode material. Additionally, LSCM conductivity is $175\,S\,cm^{-1}$ at 800 °C [20], greater than that of $Mn_{1.5}Co_{1.5}O_4$ at $90\,S\,cm^{-1}$ [23]. Good conducting compounds, such as $SrCrO_3$ and $Mn_{1.5}CrO_4$, are expected to form within the LSCM protection layer, which should prevent Cr from diffusing into the LSCF cathode [25–27]. To minimize the formation of Cr_2O_3 and Cr_3O_4, we used LSCM to form a low resistance and high electrical conductivity oxide coating on Crofer22H, and prevent poisoning of the LSCF cathode.

In this study, the Crofer22H surface was coated with $La_{0.1}Sr_{0.9}Co_{0.5}Mn_{0.5}O_{3-\delta}$ (LSCM) by screen-printing, followed by heat treatment at 800 °C for 100 h. The phase, element distribution, and microstructure of the oxidized film were analyzed in detail. Additionally, we investigated the effect of the LSCM protection layer on the electrochemical performance of the LSCF cathode.

2. Experimental

LSCM powder was prepared by citrate–EDTA complexation [29]. Ethylenediaminetetraacetic acid (EDTA, Riedel-dehaen, 98%) was mixed with 6 M NH_3 to form an NH_3–EDTA solution. $La(NO_3)_3{\cdot}6H_2O$ (Alfa Aesar, 99.0%) was added, and the mixture was gently heated and stirred. Meanwhile $Sr(NO_3)_2$ (Alfa Aesar, 99.0%), $Mn(NO_3)_2{\cdot}4H_2O$ (Fluka, 97.0%), and $Co(NO_3)_2{\cdot}6H_2O$ (J.T. Baker, 99%) were combined in a second vessel containing 6 M NH_4OH solution, and the two solutions were then mixed with stirring before citric acid (J.T. Baker, 99.8%) was added. The resulting mole ratio of EDTA:citric acid:total metal ions was 1:1.5:1. The pH was adjusted to pH 6 by addition of 6 M NH_4OH solution. The final solution was heated to 100 °C on a hotplate, and stirred until the water had evaporated, leaving a sticky gel. This gel was heated at 200 °C for 3 h and calcined at 1100 °C for 12 h to obtain the LSCM powders. The LSCM protection layer was coated on Crofer22H interconnect by screen-printing. A slurry of LSCM at a suitable viscosity for screen-printing was typically prepared by ball-milling a mixture of LSCM with ethyl cellulose-terpineol (J.T. Baker) binder. After screen printing, the LSCM/Crofer22H composite was baked at 400 °C for 3 h.

The electrical conductivity of symmetrical samples was measured continuously for 100 h at 800 °C in air, using four DC terminals. Silver was used for the metal electrodes. Data acquisition was performed using Agilent Technologies 34970A, 6645A data acquisition and switch units with a separate power supply (GWINSTEK GPS-3030DD). Fig. 1(a) shows a schematic diagram of the experimental setup. Sample ASR depends on the following relation:

$$\mathrm{ASR} = \tau_s \iota_s + \tau_o \iota_o \quad (1)$$

where τ_s and ι_s are the resistance and thickness, respectively, of the metal interconnect, while τ_o and ι_o are the resistance and oxidation thickness, of the surface oxide layer. The resistance of alloy is significantly lower than that of the surface oxide layer, and therefore, the alloy's resistance could be neglected. Therefore, the ASR of the protection layer/interconnect sample is described by the following equation:

$$\mathrm{ASR} = \tau_o \iota_o \quad (2)$$

To investigate the effect of Cr on the electrical conductivity and resistance of LSCF cathode electrode, the LSCF rectangular bar and symmetrical LSCF/$Ce_{0.8}Sm_{0.2}O_{1.9}$ (SDC, Gimat)/LSCF cells were contacted with Crofer22H and LSCM/Crofer22H respectively, as shown in Fig. 1(b) and (c), and heated at 800 °C for 100 h. Composite electrode disks comprising LSCF-30 wt.% SDC were screen printed on

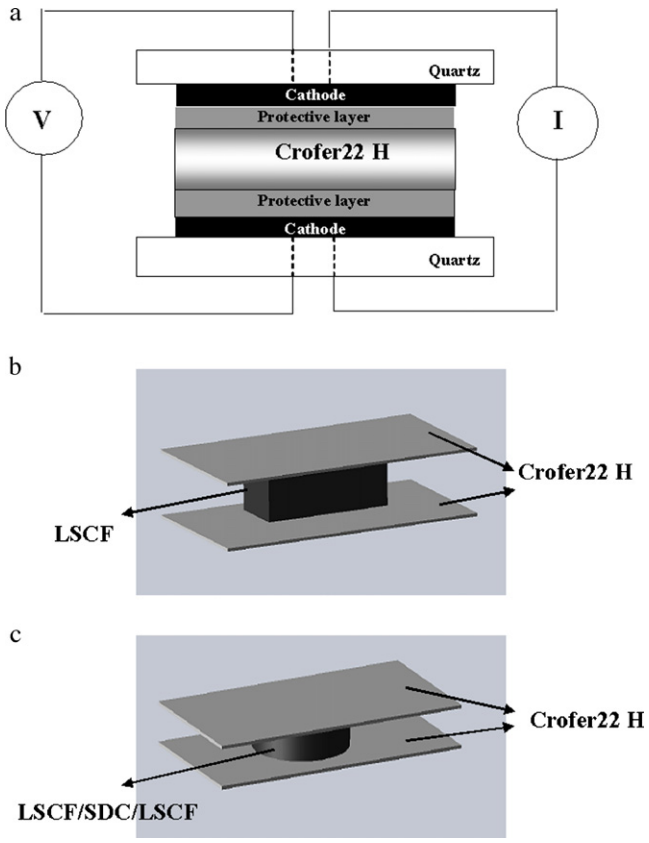

Fig. 1. (a) Schematic of ASR measurement device for with and without protective layer for Crofer22H samples. Schematic of (b) LSCF cathode and (c) LSCF/SDC/LSCF symmetry cell samples for conductivity and AC impedance measurements.

both sides to prepare symmetrical cells for use in electrochemical impedance spectroscopy (EIS). The SDC substrate disks, 10 mm in diameter and 0.5 mm thick, were prepared by solid-state sintering at 1600 °C for 4 h. A slurry at an appropriate viscosity for screen printing was typically obtained by ball-milling a mixture of 0.3 g LSCF with 0.13 g SDC powder and ethyl cellulose-terpineol binder. After screen-printing, the cells were baked at 120 °C and then sintered at 1050 °C for 5 h.

The electrical resistance of LSCF samples was measured in air using a DC four-terminal approach (Fig. 1(a)), and sample electrical conductivity was calculated from the following equation:

$$\sigma = \frac{L}{A \cdot \Omega} \tag{3}$$

where σ, electrical conductivity (S cm^{-1}), L, specimen thickness (cm), A, cross-sectional area (cm^2), Ω, resistance (ohm, Ω).

The EIS was performed using an impedance analyzer (HIOKI, 3532-50) at 30 mV, and operating at frequencies ranging from 0.01 Hz to 1 MHz, at temperatures ranging from 600 to 800 °C.

The phases present in the oxidation layers on Crofer22H and LSCM/Crofer22H following heat treatment was determined using an X-ray powder diffractometer (LabX, XRD-6000), and low grazing angle XRD (Rigaku 18 kW Rotating Anode X-ray Generator) with Ni-filtered Cu Kα radiation. Diffraction angle scanning was from 15° to 80° in 0.01° steps at a rate of 1° min^{-1}. The analyses of microstructure and element distribution were conducted using field emission scanning electron microscopy (FE-SEM) (JEOL JSM-6701F) and electron dispersive spectroscopy (EDS) (INCA HP12 3SE, UK).

3. Results and discussion

Fig. 2 shows the Glancing Angle X-ray Diffraction (GAXRD) patterns of the Crofer22H surface, the LSCF/Crofer22H interface, the LSCM/Crofer22H interface, and LSCF with LSCM/Crofer22H after heat treatment at 800 °C for 100 h. Fig. 2(a) shows that Cr_2O_3 (JCPDS 84-0315) and $(Mn_{0.98}Fe_{0.02})(Mn_{0.02}Fe_{0.48}Cr_{1.5})O_4$ (JCPDS 89-3746) oxides formed on the surface of Crofer22H during heat treatment. Fig. 2(b) shows that the presence of $SrCrO_3$ (JCPDS 20-1192), $LaCrO_4$ (JCPDS 49-1710), $CoCr_2O_4$ (JCPDS 80-1668), Cr_3O_4 (JCPDS 12-0559), $(Mn_{0.98}Fe_{0.02})(Mn_{0.02}Fe_{0.48}Cr_{1.5})O_4$, and $(Fe,Cr)_2O_3$ (JCPDS 02-1357) oxides formed at the interface between LSCF and Crofer22H. The $(Fe,Cr)_2O_3$ oxide is the main component of rusting iron, and the compound has a high electrical resistance. Thus, it is anticipated that the ASR of LSCF/Crofer22H should increase due to

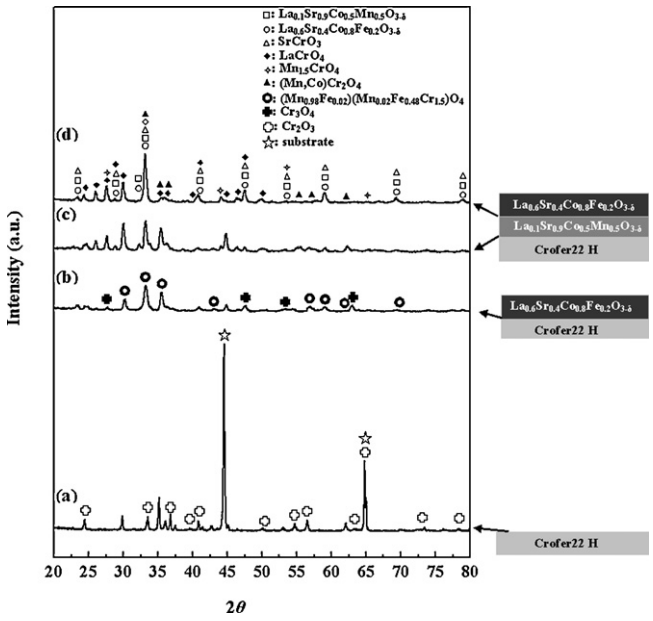

Fig. 2. GAXRD patterns after heat treatment at 800 °C for 100 h of (a) Crofer22H, (b) LSCF and Crofer22H interface, (c) LSCM and Crofer22H interface, and (d) LSCF and LSCM/Crofer22H interface.

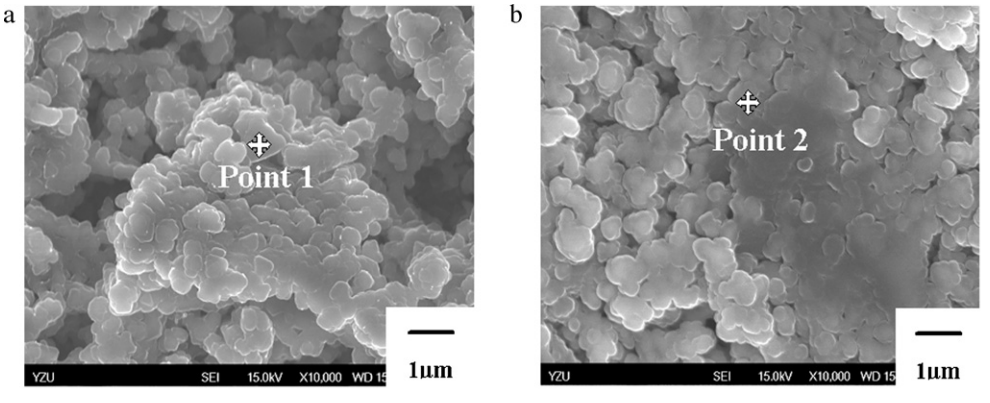

Elements	Atomic(%)
O	70.37
Cr	4.97
Fe	2.86
Co	8.48
Sr	6.38
La	6.94
Total	100

Elements	Atomic(%)	
O	63.24	
Cr	0	
Fe	2.83	(2)
Co	11.79	(8)
Sr	10.13	(4)
La	12.01	(6)
Total	100	

Fig. 3. SEM micrographs and EDS results of LSCF cathode coated (a) Crofer22H, and (b) LSCM/Crofer22H after heat treatment at 800 °C for 100 h.

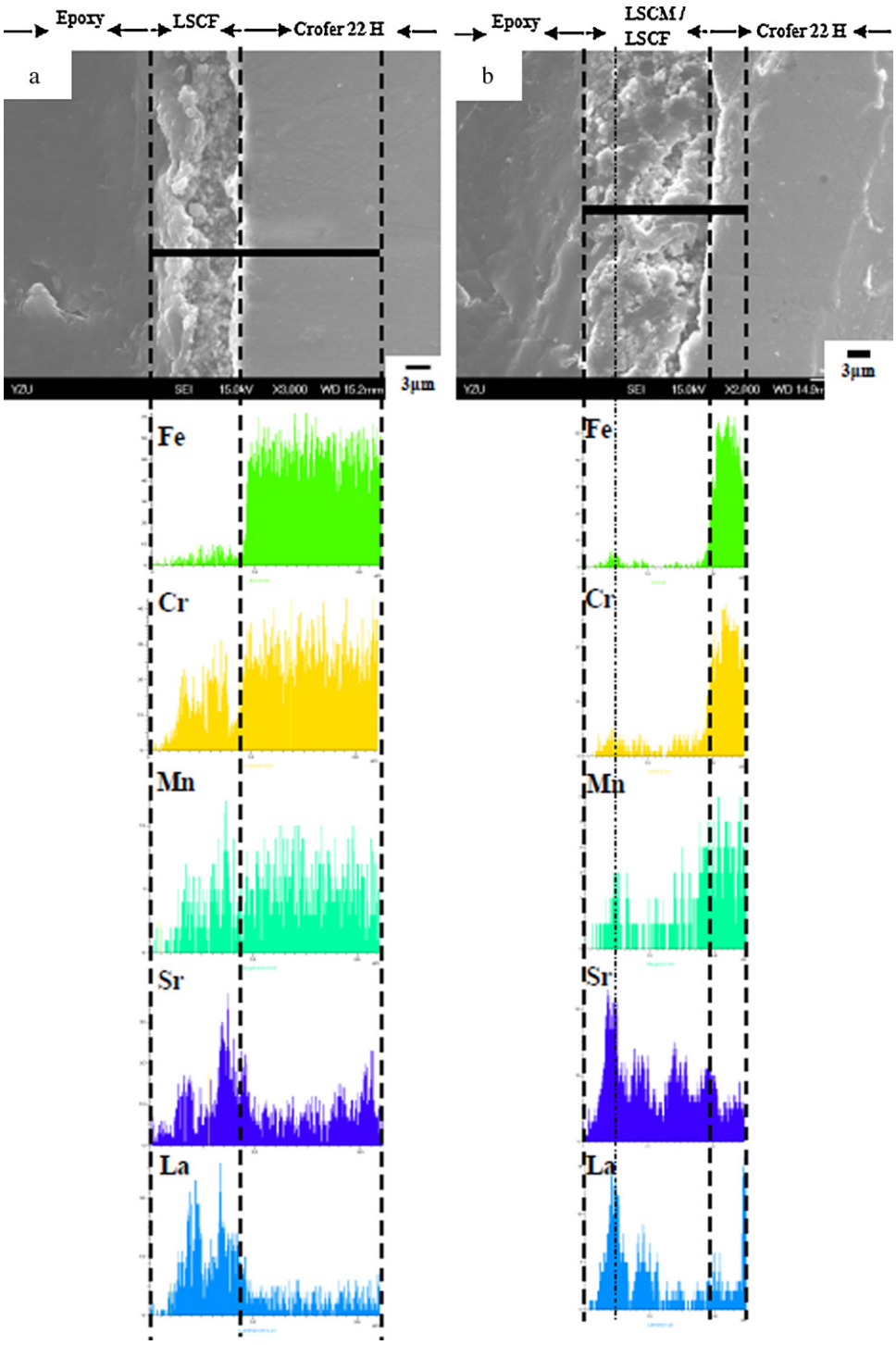

Fig. 4. SEM cross-sectional micrographs and EDS line-scans of (a) LSCF/Crofer22H, and (b) LSCF/LSCM/Crofer22H after heat treatment at 800 °C for 100 h.

the formation of $(Fe,Cr)_2O_3$ oxides. Fig. 2(c) shows phases present at the LSCM and Crofer22H interface include $SrCrO_3$, $LaCrO_4$, $Mn_{1.5}CrO_4$ (JCPDS 44-0909), $(Mn,Co)Cr_2O_4$ (JCPDS 36-0546 and 80-1668), and Cr_3O_4. The Cr_2O_3, which was apparently present at the Crofer22H surface, was not observed in this sample. Fig. 2(d) shows that phases formed at the interface between the LSCF cathode and LSCM/Crofer22H include $SrCrO_3$, $LaCrO_4$, and $Mn_{1.5}CrO_4$. None of the high electrical resistance compounds Cr_3O_4, Cr_2O_3, or $(Fe,Cr)_2O_3$ were detected. We expected that conductivity of the LSCF/LSCM/Crofer22H sample would be greater than that of LSCF/Crofer22H, and that the LSCM protection layer could prevent the LSCF cathode from poisoning by Cr evaporated from the Crofer22H [28]. The conductivity and electrochemical properties are discussed below.

There was large quantity of $(Mn, Co)Cr_2O_4$-based compounds formed at the LSCM/Crofer22H and LSCF/LSCM/Crofer22H interfaces. However, only small amount of $MnCr_2O_4$ compound formed at the LSCF and Crofer22H interface, due to the small quantity of manganese present in Crofer22H (Table 1). Therefore, the conductivity of LSCF/LSCM/Crofer22H should be much greater than that of

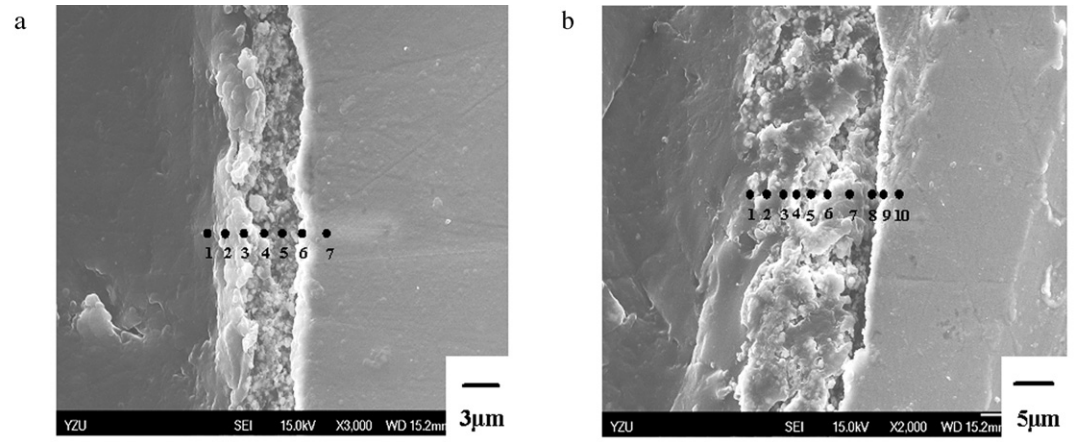

Element / Point	La(%)	Sr(%)	Co(%)	Cr(%)	Fe(%)	Cl(%)	O(%)
1	--	--	--	--	--	14.82	85.18
2	--	--	--	--	--	15.51	84.49
3	9.36	8.69	10.36	10.77	3.70	--	57.12
4	16.57	4.59	24.51	30.87	6.59	--	16.87
5	16.57	7.21	18.73	8.52	6.98	--	41.99
6	5.28	8.93	4.25	11.82	2.23	--	67.49
7	--	--	--	19.77	60.92	--	19.31

Elements / Point	La(%)	Sr(%)	Co(%)	Mn(%)	Cr(%)	Fe(%)	Cl(%)	O(%)
1	--	--	--	--	--	--	9.41	90.59
2	3.01	2.77	3.82	--	--	0.37	8.30	81.73
3	7.79	6.70	11.21	--	1.26	2.77	--	70.27
4	8.65	6.03	11.58	0.46	1.17	3.51	--	68.60
5	7.71	10.45	6.86	1.96	1.90	3.49	--	67.63
6	8.93	6.03	12.74	0.36	0.94	0.36	--	68.59
7	1.67	3.07	0.40	0.16	2.18	--	--	92.52
8	0.29	6.09	4.90	2.25	5.47	1.22	--	79.49
9	--	14.63	30.03	--	19.91	--	--	35.43
10	--	--	--	--	14.98	44.36	--	40.65

Fig. 5. SEM cross-sectional micrographs and EDS point-scans of (a) LSCF/Crofer22H, and (b) LSCF/LSCM/Crofer22H after heat treatment at 800 °C for 100 h.

LSCF/Crofer22H because of the formation of highly stable and conductive $MnCr_2O_4$. Additionally, trivalent Cr in $(Mn, Co)Cr_2O_4$ would not diffuse into the LSCF cathode by either solid-state or gaseous diffusion mechanisms.

Fig. 3 shows surface morphology micrographs and EDS results for the LSCF cathode coated on both Crofer22H and LSCM/Crofer22H after heat treatment at 800 °C for 100 h. The EDS results show that 4.97% Cr was present in the LSCF/Crofer22H sample; however, no Cr was detected in the LSCF/LSCM/Crofer22H sample. It was intended that the LSCM protection layer would prevent Cr diffusion and poisoning of the LSCF electrochemical

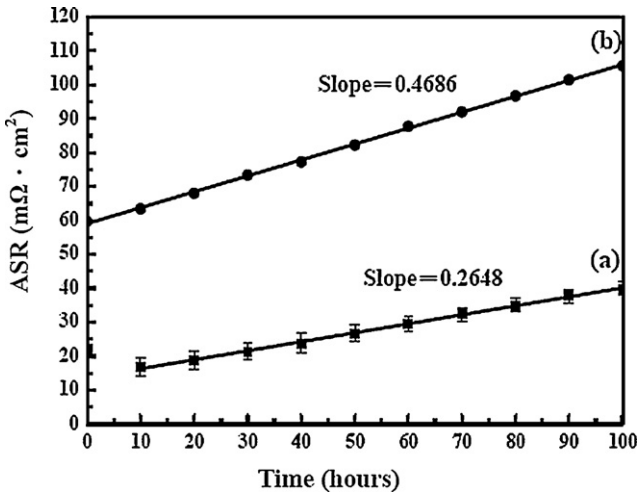

Fig. 6. Variation in ASR for (a) LSCF/LSCM/Crofer22H, and (b) LSCF/Crofer22H at 800 °C for 100 h.

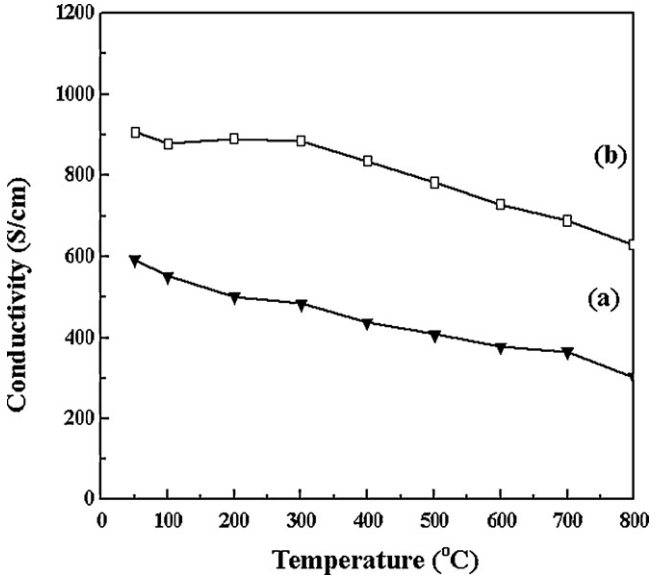

Fig. 7. Conductivity of LSCF cathode contacting with (a) Crofer22H, and (b) LSCM/Crofer22H after heat treatment at 800 °C for 100 h, as a function of temperature.

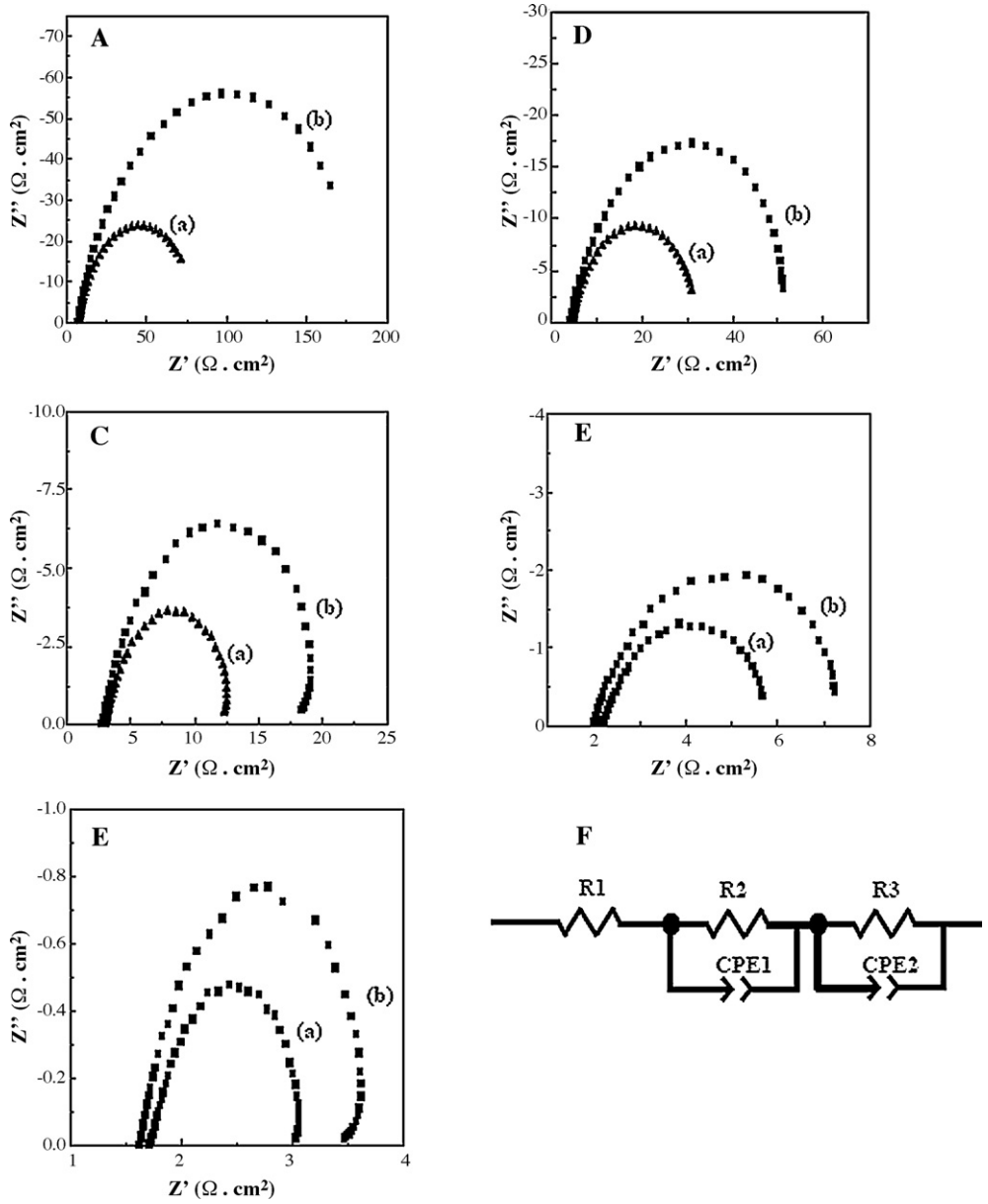

Fig. 8. Impedance spectra of (a) LSCF/LSCM/Crofer22H/LSCF, and (b) LSCF/Crofer22H/LSCF symmetry cells and measured at (A) 600 °C, (B) 650 °C, (C) 700 °C, (D) 750 °C, (E) 800 °C. (F) depicts the equivalent circuit for fitting the impedance spectra.

properties. However, the surface EDS results depend on the thickness of the LSCF and LSCM layers, so we carried out EDS cross-section line-scans of samples to confirm the elemental distribution. Fig. 4 shows the SEM cross-section micrographs and EDS line-scan results for LSCF/Crofer22H and LSCF/LSCM/Crofer22H samples. The figure shows that Cr did not diffuse to the LSCF cathode, and that the LSCM protection layer effectively prevented Cr ion diffusion. However, in the absence of an LSCM protection layer, the Cr apparently diffused into the LSCF layer.

To investigate the Cr distribution in detail, we conducted EDS point-scan analysis of sample cross-sections. In Fig. 5(a), points 1 and 2 result from epoxy resin, and point 7 is the Crofer22H interconnect. The points 3–6 are from the LSCF layer. We found that high Cr concentrations in the LSCF cathode contacting Crofer22H. Apparently, Cr had diffused from the Crofer22H interconnect to the LSCF cathode. According to the XRD pattern shown in Fig. 2(b), the main phases are $(Mn_{0.98}Fe_{0.02})(Mn_{0.02}Fe_{0.48}Cr_{1.5})O_4$ and $(Fe,Cr)_2O_3$. These are compounds with high electrical resistance. In Fig. 5(b), points 1 and 2 are respectively, epoxy resin and the LSCF cathode, and point 10 is the Crofer22H interconnect. Cr was not detected in the LSCF outer layer (point 2). Point 5 represents the LSCF and LSCM interface. The interface contains greater concentration of Sr, Cr, and Mn compared to that represented by points 4 and 6. We suggest that large amounts of $SrCrO_3$ and $Mn_{1.5}CrO_4$, and a small quantity of $LaCrO_4$ formed at both LSCF/LSCM and LSCM/Crofer22H interfaces. The points 8 and 9 represent the oxide layer in Crofer22H. Cr tended to react with Sr and Mn to form $SrCrO_3$ and $Mn_{1.5}CrO_4$ at the LSCM/Crofer22H interface, which is consistent with the XRD pattern shown in Fig. 2(d). Accordingly, elemental distribution results showed that the LSCM protection layer is effective in preventing Cr diffusion into the LSCF cathode. The concentration of Cr in LSCF coated onto LSCM/Crofer22H was much less than that in LSCF coated onto Crofer22H.

Fig. 6 shows the ASR of LSCF/LSCM/Crofer22H and LSCF/Crofer22H samples after heat treatment at 800 °C for 100 h. The figure clearly shows that the ASR values of the LSCF/Crofer22H

Table 2
Resistance values of (a) LSCF/LSCM/Crofer22H/LSCF and (b) LSCF/Crofer22H/LSCF symmetry cells as a function of temperature.

Temperature	Impedance			
	R2 ($\Omega\,cm^2$)		R_{total} ($\Omega\,cm^2$)	
600 °C (a)	10.50	172.86	183.36	↓60%
600 °C (b)	1.67	72.46	74.13	
650 °C (a)	0.64	50.66	51.30	↓46%
650 °C (b)	0.02	27.58	27.60	
700 °C (a)	0.02	18.31	18.33	↓43%
700 °C (b)	0.002	10.49	10.49	
750 °C (a)	0.56	4.97	5.53	↓31%
750 °C (b)	0.25	3.54	3.79	
800 °C (a)	0.15	1.97	2.12	↓33%
800 °C (b)	0.14	1.27	1.41	

increase from 60 to 105 $m\Omega\,cm^2$ during the heat treatment, and the increase in the ASR slope is 0.4686 $m\Omega\,cm^2\,h^{-1}$. The LSCF/LSCM/Crofer22H sample ASR value only increases from 17 to 40 $m\Omega\,cm^2$ during heating, the increases in the ASR slope is 0.2648 $m\Omega\,cm^2\,h^{-1}$. Comparing the ASR values and slopes of LSCF/LSCM/Crofer22H with LSCF/Crofer22H shows that the LSCM protection layer can efficiently protect the LSCF cathode from poisoning by Cr, and retain low electrical resistance after long periods of heating.

To investigate the effect of Cr poisoning on the LSCF cathode's electrical and electrochemical properties, we used a 4-probe DC method and AC impedance spectroscopy to measure the conductivity, and polarization of the LSCF cathode electrodes while contacting with Crofer22H and the LSCM/Crofer22H interconnect during heating. The LSCF electrode conductivity, in contact with LSCM/Crofer22H, fell in the range of 907–601 $S\,cm^{-1}$ from 50 to 800 °C (Fig. 7). This range that is about 1.5 times greater than that of the LSCF electrode (593–314 $S\,cm^{-1}$) when in contact with Crofer22H. This finding apparently demonstrated that LSCF in the absence of the LSCM coated layer, will be poisoned by Cr diffusion from the Crofer22H interconnect, due to the formation of Cr_3O_4, $(Fe,Cr)_2O_3$ and $(Mn_{0.98}Fe_{0.02})(Mn_{0.02}Fe_{0.48}Cr_{1.5})O_4$ oxides. The LSCM protection layer prevents Cr diffusion into the LSCF cathode; therefore, LSCF conductivity remains high at 800 °C for 100 h.

The charge transfer and oxygen ion diffusion-polarization of LSCF cathodes, contacting with Crofer22H and LSCM/Crofer22H, were measured by AC impedance spectroscopy in the temperature range 600–800 °C. The equivalent circuit [30], shown in Fig. 8(F), was used to fit the impedance spectra. R1 includes the electrolyte, electrode, and lead ohmic resistance; R2 corresponds to resistance arising during the charge transfer process. R3 corresponds to the adsorption-desorption of oxygen, oxygen diffusion at the gas–cathode interface, and surface diffusion of intermediate oxygen species. Table 2 and Fig. 9 are the resistance values of LSCF/LSCM/Crofer22H/LSCF and LSCF/Crofer22H/LSCF symmetry cells as a function of temperature. These results indicate that R_{total} for the sample coated with LSCM, is much smaller than it is for the uncoated sample. The resistance to diffusion of oxygen ion becomes serious when the LSCF was poisoned by Cr, and leads to the conversion of oxygen molecules into oxygen ions; oxygen ion diffusion then becomes more difficult. The extent of oxygen ion diffusion into the electrolyte significantly decreases, resulting in a drastic decline in SOFC power efficiency. The polarization of the LSCM coated LSCF cathode contacting with Crofer22H was much smaller than that of uncoated LSCF cathode contacting Crofer22H, at low temperatures in particular.

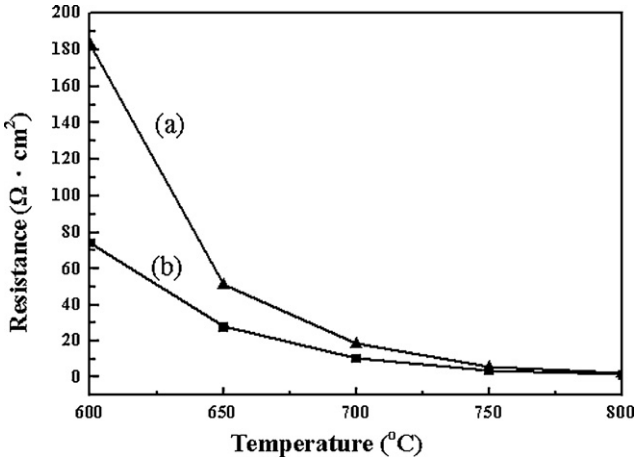

Fig. 9. Resistance of (a) LSCF/LSCM/Crofer22H/LSCF, and (b) LSCF/Crofer22H/LSCF symmetry cells measured at 600–800 °C.

4. Conclusions

The ASR of LSCF/LSCM/Crofer22H increased from 17 to 40 $m\Omega\,cm^2$, which was a much lower increase than that seen for LSCF/LSCM samples. Additionally, the conductivity of LSCF contacting LSCM/Crofer22H at 800 °C was about 601–907 $S\,cm^{-1}$, which was much higher than that for LSCF contacting Crofer22H. The resistance to oxygen charge transfer and oxygen ion diffusion by the LSCF cathode contacting LSCM/Crofer22H at 800 °C was significantly lower than that of LSCF contacting with Crofer22H, especially in the lower temperature range of 600–700 °C. These results suggest that the LSCM layer was effective at preventing Cr diffusion or evaporation from the Crofer22H interconnect into the LSCF cathode, and so prevent the reduction of oxygen and subsequent oxygen ion diffusion. XRD and EDS results confirm that the LSCM coating layer could produce high conductivity oxides, including $SrCrO_3$, $LaCrO_4$, $Mn_{1.5}CrO_4$, and $(Mn,Co)Cr_2O_4$ and prevent the formation of large quantities of low conductivity Cr_3O_4, $(Mn_{0.98}Fe_{0.02})(Mn_{0.02}Fe_{0.48}Cr_{1.5})O_4$, and $(Fe,Cr)_2O_3$. We conclude that the performance of LSCF/LSCM/Crofer22H is superior to that of LSCF/Crofer22H.

Acknowledgements

The authors acknowledge financial support provided by the National Science Council in Taiwan, under Contract Nos. NSC 100-3113-E-155-001 and NSC 100-3113-E-006-011.

References

[1] N.Q. Minh, J. Am. Ceram. Soc. 76 (1993) 563–588.
[2] M.R. Ardigo, A. Perron, L. Combemale, O. Heintz, G. Caboche, S. Chevalier, J. Power Sources 196 (2011) 2037–2045.
[3] Z.H. Bi, J.H. Zhu, J.L. Batey, J. Power Sources 195 (2010) 3605–3611.
[4] X. Montero, F. Tietz, D. Stover, M. Cassir, I. Villarreal, J. Power Sources 188 (2009) 148–155.
[5] Z. Yang, G. Xia, P. Singh, J.W. Stevenson, J. Power Sources 155 (2006) 246–252.
[6] Y. Liu, D.Y. Chen, Int. J. Hydrogen Energy 34 (2009) 9220–9226.
[7] S.H. Kim, J.Y. Huha, J.H. Jun, J.H. Jun, J. Favergeon, Curr. Appl. Phys. 10 (2010) S86–S90.
[8] S.P. Simner, M.D. Anderson, G.G. Xia, Z. Yang, L.R. Pederson, J.W. Stevenson, J. Electrochem. Soc. 152 (4) (2005) A740–A745.
[9] G.Y. Lau, M.C. Tucker, C.P. Jacobson, S.J. Visco, S.H. Gleixner, L.C. DeJonghe, J. Power Sources 195 (2010) 7540–7547.
[10] C.J. Fu, K.N. Sun, X.B. Chen, N.Q. Zhang, D.R. Zhou, Electrochim. Acta 54 (2009) 7305–7312.
[11] J. Wu, R.S. Gemmen, A. Manivannan, X. Liu, Int. J. Hydrogen Energy 36 (2010) 4525–4529.
[12] J. Wu, C.D. Johnson, R.S. Gemmen, X. Liu, J. Power Sources 189 (2009) 1106–1113.
[13] H. Hwang, G.M. Choi, J. Electroceram. 22 (2009) 67–72.
[14] M.J. Tsai, C.L. Chu, S. Lee, J. Alloys Compd. 489 (2010) 576–581.
[15] L.T. Wilkinson, J.H. Zhu, J. Electrochem. Soc. 156 (8) (2009) B905–B912.

[16] E. Tondo, M. Boniardi, D. Cannoletta, M.F. de Riccardis, B. Bozzini, J. Power Sources 195 (2010) 4772–4778.
[17] W. Huang, S. Gopalan, U.B. Pal, S.N. Basu, ECS Trans. 13 (26) (2008) 405–411.
[18] S. Molin, B. Kusz, M. Gazda, P. Jasinski, J. Solid State Electrochem. 13 (2009) 1695–1700.
[19] J.J. Choi, J. Ryu, B.D. Hahn, W.H. Yoon, B.K. Lee, D.S. Park, J. Mater. Sci. 44 (2009) 843–848.
[20] Z. Yang, G.G. Xia, X.H. Li, J.W. Stevenson, Int. J. Hydrogen Energy 32 (2007) 3648–3654.
[21] Z. Yang, G.G. Xia, G.D. Maupin, J.W. Stevenson, Surf. Coat. Technol. 201 (2006) 4476–4483.
[22] J. Yoo, S.K. Woo, J.H. Yu, S. Lee, G.W. Park, Int. J. Hydrogen Energy 34 (2009) I542–I547.
[23] Z. Yang, G. Xia, Z. Nie, J. Templeton, J.W. Stevenson, Electrochem. Solid State 11 (8) (2008) B140–B143.
[24] X. Chen, P.Y. Hou, C.P. Jacobson, S.J. Visco, L.C. de Jonghe, Solid State Ionics 176 (2005) 425–433.
[25] F. Tietz, H.P. Buchkremer, D. Stover, Solid State Ionics 152–153 (2002) 373–378.
[26] I. Yasuda, T. Hikita, J. Electrochem. Soc. 140 (1993) 1699–1704.
[27] P. Duran, J. Tartaj, F. Capel, C. Moure, J. Eur. Ceram. Soc. 24 (2004) 2619–2629.
[28] Y. Aoki, H. Konno, H. Tachikawa, J. Mater. Chem. 11 (2001) 1214–1221.
[29] I.M. Hung, C.Y. Liang, C.J. Ciou, Y.C. Lee, Ceram. Int. 36 (2010) 1937–1943.
[30] Q.A. Huang, R. Hui, B. Wang, J. Zhang, Electrochem. Acta 52 (2007) 8144–8164.